

Polarization Dependence of Aragonite Calcium L-Edge XANES Spectrum Indicates *c* and *b* Axes Orientation

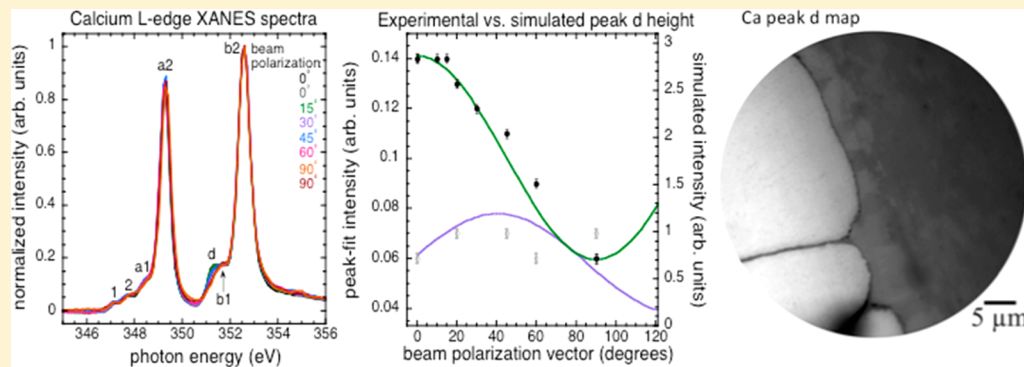
Rebecca A. Metzler*,† and Peter Rez^{‡,§}

†Department of Physics and Astronomy, Colgate University, 13 Oak Dr., Hamilton, New York 13346, United States

‡Department of Physics, Arizona State University, P.O. Box 871504, Tempe, Arizona 85287, United States

§Department of Structural Biology, Weizmann Institute of Science, Rehovot 7610001, Israel

Supporting Information



ABSTRACT: Calcium carbonate minerals are frequently found in biomineral structures and are the predominant mineral in invertebrates. While there are several calcium carbonate polymorphs, aragonite and calcite are the two most commonly found in biogenic systems. Currently, calcium L-edge X-ray absorption near-edge structure (XANES) spectra are used to distinguish between different calcium carbonate polymorphs, including calcite and aragonite, while oxygen and carbon K-edge XANES spectra are often used to determine the *c* axis orientation of a given calcium carbonate crystal. By doing a full analysis of the calcite and aragonite calcium L-edge XANES spectrum for both geologic and biogenic systems, we were able to show that aragonite has a polarization-dependent peak while calcite does not. Analysis based on both multiplet models and density functional calculations show how the polarization dependence arises from directional bonds between the calcium and oxygen atoms within aragonite. These data not only enable an interpretation of the aragonite calcium L-edge XANES spectrum but also the ability to determine the orientation of the *c* and *b* axes of aragonite crystals within a biomineral sample.

INTRODUCTION

Calcium carbonate minerals are the predominant mineral component in invertebrate biomineral structures found in the shells of mollusks, gastropods, and cephalopods as well as trilobite eye lenses and barnacle exoskeletons.¹ The most common nonhydrated calcium carbonate (CaCO_3) polymorphs are aragonite and calcite, due in part to their high thermodynamic stability.¹ One way in which to probe the local chemistry occurring within biomineral structures and the calcium carbonate polymorphs that make up the structures is to use X-ray absorption near-edge structure (XANES) spectroscopy.^{2–6} Much work has been done to carefully document and explore the spectral features found at the XANES carbon K-edge in calcite and aragonite and the oxygen K-edge in several calcium carbonates, making it possible to determine the *c* axis orientation,^{3,4,6–8} which has led to a deeper understanding of biomineral structures and formation mechanisms.^{2,4,5,9–11} However, there are still unanswered questions in the interpretation of features in the calcium L-edge XANES spectrum of aragonite. Here we undertake a careful analysis of

the calcium L-edge XANES spectra of calcite and aragonite, characterizing all spectral features found in both spectra, and demonstrate the ability of the calcium L-edge XANES spectrum to indicate *c* and *b* axes orientation for aragonite crystals.

While the calcite and aragonite calcium carbonate polymorphs are the two most prevalent polymorphs in biomineral structures and are even occasionally found within a single biomineral structure, the crystalline structure of the two polymorphs are quite different and lead to different local coordination chemistries, which is detectable by XANES spectroscopy. Calcite has alternating Ca^{2+} cation and CO_3^{2-} ion layers that stack along the (0001) axis, resulting in a structure in which the Ca^{2+} is coordinated with six oxygen atoms from the surrounding CO_3^{2-} groups.^{12–14} In aragonite, the Ca^{2+} cations and CO_3^{2-} ions are still in alternating layers along the (001) direction, but the CO_3^{2-} ions are staggered and

Received: April 11, 2014

Revised: May 19, 2014

Published: May 21, 2014

tilted $\sim 2^\circ$ out of the (001) plane; this results in the Ca^{2+} ions having a 9-fold coordination with oxygen.^{12,13,15} These differences in the crystal structure lead to distinct XANES spectra, as shown at the calcium L-edge in Figure 1 and in

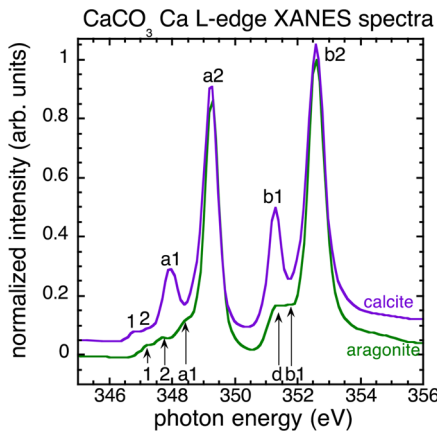


Figure 1. Calcium L-edge XANES spectrum of calcite (purple) and aragonite (green) with the distinct regions of the spectra labeled 1, 2, a1 and d, b1 per Fleet et al.¹²

previous articles.^{2,12,16–18} The two polymorphs are distinguished through the spectral peaks in the crystal field regions, labeled 1, 2, a1, d, and b1. The calcium L-edge XANES spectrum for calcite has been fully analyzed, and each peak has been accounted for both through group theory arguments¹² and through simulations based on multiplet calculations.¹³ While the aragonite calcium L-edge XANES spectrum has been documented several times experimentally, theoretical analysis of the spectrum has not been able to explain all of the spectral peaks observed, leading to the suggestion that the unexplained peaks, one not observed in Figure 1 and peak d, are due to calcite contamination of the sample.¹² In addition, due to the lower symmetry of aragonite, it is not possible to perform accurate multiplet calculations, making it difficult to match simulation exactly with experiment.¹³

While the lower symmetry of aragonite makes exact simulations untenable, theory predicts that this lower symmetry should make the calcium L-edge XANES spectrum polarization dependent, while the calcite spectrum should not be polarization dependent due to its higher symmetry.^{19,20} We used this fact to experimentally examine the polarization dependence of the calcite and aragonite calcium L-edge XANES spectra, enabling us not only to provide an explanation for the polarization dependence of peak d in the aragonite spectrum but also to make use of this polarization dependence to probe biomineral microstructures.

■ EXPERIMENTAL METHODS

Sample Preparation. In our experiments, the geologic aragonite sample originated from Morocco and the geologic calcite sample was purchased from MTI Corporation. The biogenic aragonite and calcite samples are from the shell of a marine oyster, *Pinctada margaritifera*, collected from the Philippines and purchased from Conchology, Inc.

Geologic Samples. The geologic aragonite sample was chiseled from a large aragonite crystal cluster. The aragonite crystal was cleaned in a series of three baths for 20 min each to remove any organic contamination from the mineral: trichloroethane, acetone, and ethanol.³ The crystal was then placed in

epoxy so that the c axis was located in the plane of the sample and polished with decreasing grits with the smallest being a 50 nm alumina slurry. After cleaning with ultrapure water, the sample was differentially coated with 1 nm of platinum in the region of interest and 40 nm in the surrounding region.²¹

The geologic calcite sample was provided by MTI Corporation, where it was processed, cleaned, and cut so the c axis was located in-plane. The sample was differentially coated prior to XANES analysis.

The crystallographic orientation of both geologic crystals was confirmed with electron backscatter detection (EBSD) following X-PEEM experiments with the c axis of both crystals being less than 5° out of the crystal plane. When the c axis for the aragonite sample was in the horizontal orientation (Figure 2A), the a axis was vertical and 53° out of the sample plane, while the b axis was vertical and 37° out of the sample plane. The vertical orientation of the aragonite crystal resulted from a 90° rotation of the sample (Figure 2B). When the c axis for the calcite sample was in the horizontal orientation (Figure 2C), the a axis was perpendicular to the sample and the b axis was vertical and 30° out of the sample surface. As with the aragonite crystal, a 90° rotation of the calcite crystal resulted in the vertical orientation shown in Figure 2D. These angles were used to orient the aragonite crystal for simulations.

Biogenic Samples. The biogenic samples were chiseled from a larger specimen, embedded in epoxy, and polished down to the region of interest, namely a cross section of the *Pinctada margaritifera* shell in which both the calcitic prismatic layer and aragonitic nacre layer were exposed. At this point, the samples were prepared in an identical manner to the geologic samples.

■ DATA ACQUISITION

XANES and X-PEEM at the CLS on the SM Beamline. Calcium L-edge spectra were acquired on the SM beamline at the Canadian Light Source (CLS) with the X-PEEM microscope for all three samples: geologic aragonite, geologic calcite, and the combined biogenic calcite and aragonite. The SM beamline is equipped with an elliptically polarized undulator, which allows the user to change the incoming beam's polarization, enabling polarization studies to be conducted on a single region of the sample without moving the sample, as done here. For all experiments, the samples were mounted vertically and the synchrotron beam was incident on the sample at a 16° grazing angle. To encompass the full angle range described here and to check for consistency, data were acquired on the same geologic sample at two different orientations, one with the c axis in-plane and in the x direction, "horizontal", and one with the c axis in-plane and in the $-z$ direction, "vertical" (90° rotation with respect to the first orientation) (Figure 2).

Data was acquired from each sample over an energy range of 338–370 eV with an energy step of 0.5 eV from 338 to 345 and 357–370 and 0.1 eV elsewhere.

Spectral Analysis and Normalization. All spectra were extracted from a single, uniform region within an X-PEEM image taken at the carbon or oxygen π^* peak, as such an image is known to highlight c axis orientation in calcite and aragonite.^{3,4,7} Thus, for the biogenic calcite and biogenic aragonite, care was taken to extract spectra from a single co-oriented portion of the prism or a single co-oriented stack of nacre tablets. All spectra for a single sample were simultaneously normalized to ensure any spectral variations were not normalization artifacts. All spectra were aligned with a fifth-order polynomial to ensure any beam intensity variations were

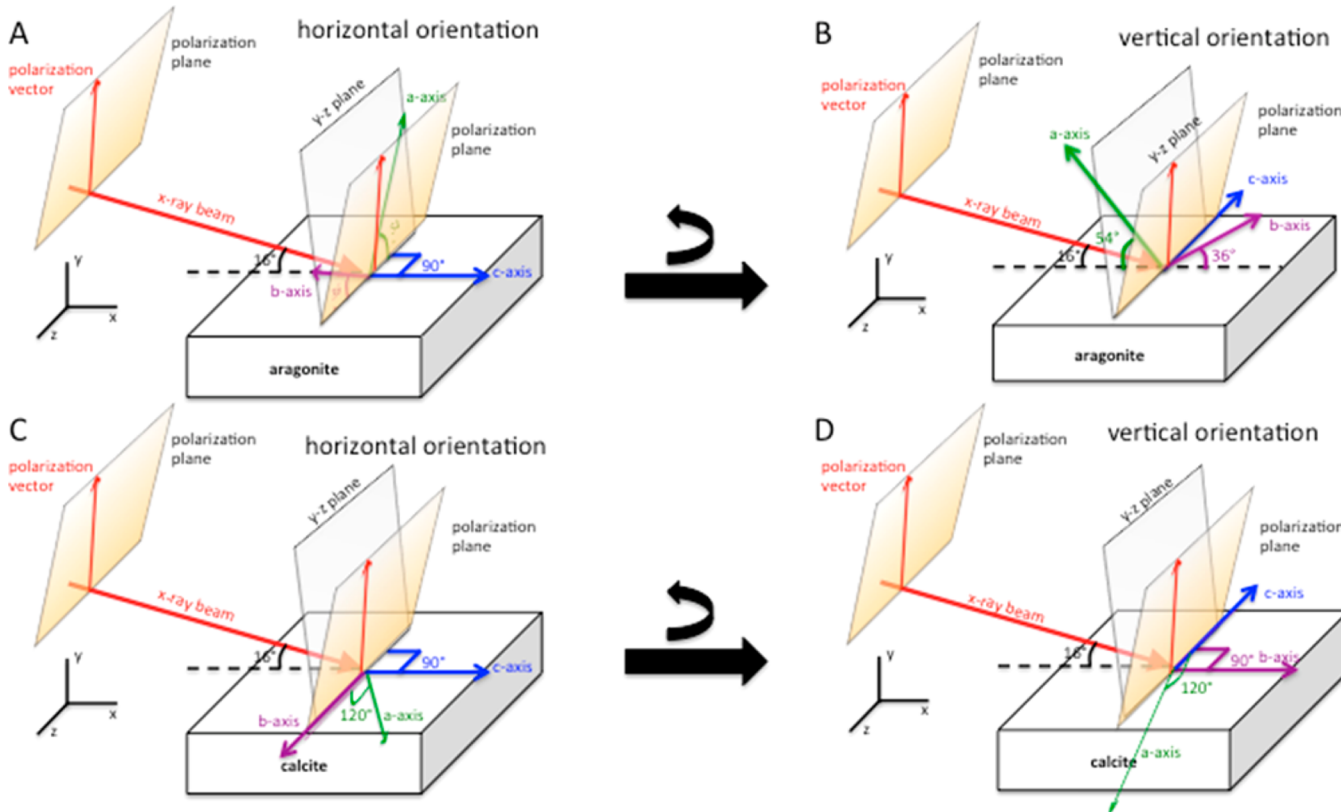


Figure 2. Experimental setup in the X-PEEM microscope at the CLS, depicting each of the two experimental arrangements for both geologic aragonite and geologic calcite single crystals. The incoming X-ray beam (red) is in the x direction and 16° above the sample surface (white) in the y direction. The polarization of the beam can be varied in the orange-colored plane through the use of the elliptically polarized undulator (EPU), resulting in a linearly polarized beam polarized at a particular angle (red arrow). As shown in the diagram, as the beam comes in at a 16° angle, the polarization plane when it reaches the sample is 16° off the $y-z$ plane. (A) In the original “horizontal” orientation of the geologic aragonite crystal, the c axis is in the plane of the sample in the x direction; the a and b axes are in the $y-z$ plane of the sample, with the a axis 54° above the sample plane (in the y direction) and the b axis 36° above the sample plane (in the x direction). To get to (B), the second “vertical” orientation of the geologic aragonite crystal, the sample was rotated by 90° , as indicated by the arrows, resulting in the c axis being in the plane of the sample in the $-z$ direction and the a and b axes being in the $x-y$ plane of the sample, with the a axis 54° above the sample plane (in the y direction) and the b axis 36° above the sample plane (in the x direction). (C) The geologic calcite crystal was oriented such that the “horizontal” position was with the c axis in the x direction (as with the geologic aragonite), and the a and b axes were oriented in the $+z$ direction and in the $y-z$ plane such that the a axis pointed down at an angle of 60° from the $-z$ and 120° from the b axis. (D) The “vertical” orientation of the geologic calcite crystal after being rotated by 90° , resulting in the c axis in the $-z$ direction, and the b axis in the $+x$, and the a axis pointing down at a 60° angle from the $+z$.

removed and normalized so that the pre-edge was 0 and the L_2 peak intensity was 1. In addition, all spectra were shifted to place the L_2 peak at 352.6 eV.^{2,16}

Peak fitting was done for all spectra, as presented in the Supporting Information. The spectra were fit with two arctangents, representing the step potential for both the L_2 and L_3 edges, and either six gaussians for calcite or seven gaussians for aragonite, representing each of the peaks visible in the spectrum. Such peak fitting allowed for a quantitative analysis of peak height and width. (Peak fitting coefficients are presented in Tables S1–S4 of the Supporting Information.)

Theory and Calculation Methods. The CTM4XAS code (version 3a) was used to model the effects of multiplet splitting on the Ca L_{23} white lines (intense main peaks). Viewing aragonite down the [100] (see Figure 3) shows an approximate 4-fold symmetry. The code starts by considering allowed atomic multiplet transitions, and then projects these to octahedral symmetry, point group O_h , and subsequently considers a reduced tetrahedral symmetry point group D_{4h} or C_{4v} . Following Rez and Blackwell, the octahedral crystal field

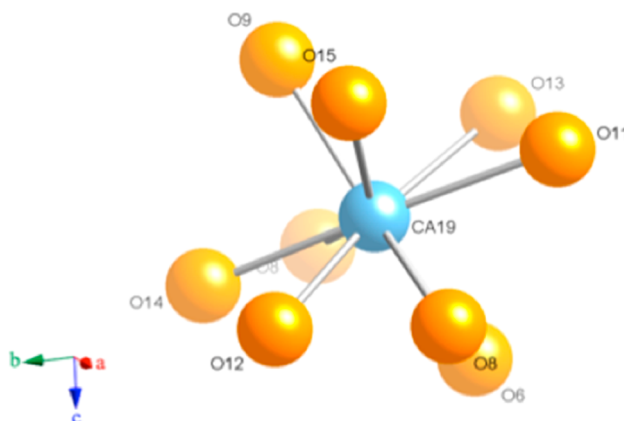


Figure 3. View of local environment of a calcium atom (blue) in aragonite showing approximate tetragonal symmetry.

splitting 10 Dq was set to 1.15 eV , and the tetrahedral distortion field Dt was 0.1 eV .¹³

To explore hybridization of unoccupied orbitals, the VASP electronic structure code²² was used to calculate the local

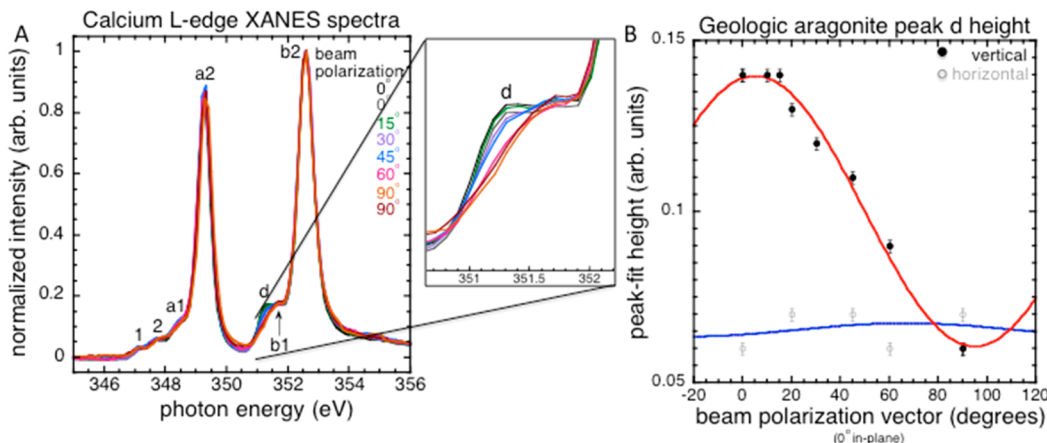


Figure 4. (A and B) Aragonite calcium L-edge XANES spectrum exhibits a distinct polarization dependence. (A) Spectra collected from a single geologic aragonite crystal (in the orientation shown in Figure 2B, *c* axis in $-z$) as the angle between the crystal and the beam polarization vector was changed demonstrates the polarization dependence of peak d at 351.3 eV. A magnified view of the peak d region illustrates this dependence with peak d intensity being high when the angle between the polarization vector and the crystal is small and small when the angle is large. This relationship is highlighted in (B) when graphing the peak-fit intensity of peak d in both sample orientations (Figure 2, panels A and B) as a function of beam polarization. Both sets of data were fit with a \cos^2 relationship. The remainder of the peaks do not show polarization dependence and thus were not included for clarity.

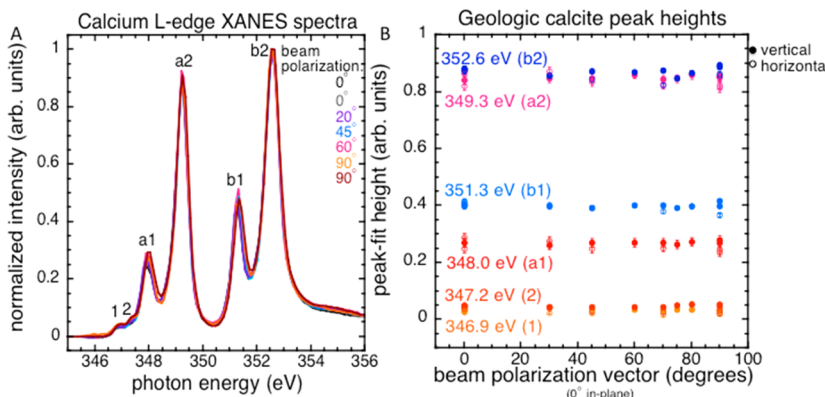


Figure 5. (A) Calcium L-edge XANES spectrum of geologic calcite appears independent of (B) the incoming synchrotron beam's polarization vector. Data was collected from a single geologic calcite crystal as the angle between the crystal and the polarization vector of the beam was varied. All variation observed between (A) spectra at different angles appears to be random and largely within the average variation observed between spectra acquired at the same angle. (B) Graphing the peak-fitted peak intensities as a function of beam polarization emphasizes this point, as there is no obvious trend for any of the peaks. Therefore, it is concluded that no peak in the calcite spectrum is polarization dependent.

density of states at each atomic site. The crystal structure from de Villiers (1971) was relaxed using the conjugate gradient scheme to achieve a total energy difference of no more than 10^{-4} eV. A $9 \times 9 \times 7$ grid of *k* points was used, and the pseudopotentials were taken as the generalized gradient (GGA) form of the Projector Augmented Wave (PAW) potentials. The relaxed cell had dimensions 5.65, 4.94, and 7.92 Å. Atom displacements were less than 0.01 in fractional coordinate positions. Projected densities of states were calculated from the relaxed structure within a radius of 1 Å for the oxygen atoms and 1.2 Å for the Ca atoms.

RESULTS

Figure 4 presents data collected when varying the angle between the beam's polarization vector and a geologic aragonite crystal. Figure 4A presents spectra collected at 7 different angles for the vertical orientation of the crystal, when the *c* axis is in the $-z$ direction (Figure 2B). The spectra in Figure 4A exhibit the 6–7 peaks characteristic of the aragonite polymorph at the calcium L-edge, with the peak at 351.3 eV (peak d) that appears

and disappears based upon the angle between the aragonite crystal and the polarization vector, indicating that the aragonite spectrum is polarization dependent. The variation of the 351.3 eV peak (peak d) intensity can be seen more clearly in a magnified version of Figure 4A, with peak d being most intense when the beam polarization vector is in the plane of the crystal (0°) for this particular orientation, aligning it with the *c* axis of the aragonite crystal. These trends can be more clearly seen in Figure 4B where peak d height is graphed as a function of the beam polarization vector for both horizontal and vertical orientations of the aragonite crystal. As shown in Figure 4B, when the crystal was oriented in the vertical position such that its *c* axis was in the $-z$ direction (●) there was larger variation of the peak d height than when the crystal was oriented in the horizontal position with its *c* axis in the *x* direction (○). The data from both orientations were fit with a \cos^2 , shown in red for the vertical data and blue for the horizontal, with a relationship of

$$I = I_0 + \alpha \cos^2(\text{beam angle} + \gamma)$$

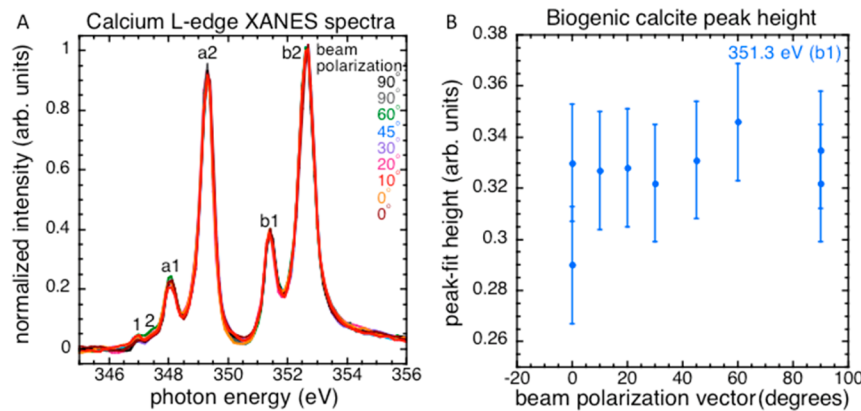


Figure 6. Calcium L-edge XANES spectra (A) extracted from a uniform region of a *Pinctada margaritifera* calcitic prism demonstrate that the biogenic calcite spectrum is remarkably similar to the geologic calcite, exhibiting all of the same peaks as the geologic calcite spectrum, and that the biogenic spectrum, similar to calcite, is not polarization dependent. Graphing the peak intensity of peak b1 at 351.3 eV as a function of the beam polarization vector, as the exact angle between the polarization and biogenic calcite is unknown, emphasizes the variation observed in the peak and the lack of correlation between peak intensity and beam polarization. The remainder of the peaks exhibit a similar behavior, thus only the 351.3 eV peak was plotted for clarity and for comparison against aragonite.

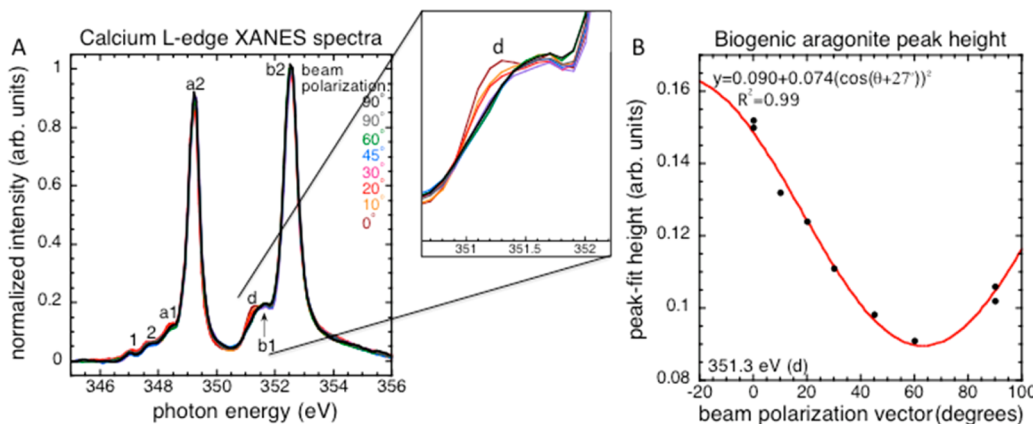


Figure 7. (A) Calcium L-edge XANES spectra extracted from a single stack of co-oriented aragonite nacre tablets from *Pinctada margaritifera* emphasizes the similarity between the geologic and biogenic aragonite spectra, with both spectra exhibiting the same peaks and the same polarization dependence, as highlighted in the magnified view of the peak d region. (B) Graphing the peak-fit peak d intensity as a function of beam polarization vector also exhibits a cosine-squared relationship as observed in geologic aragonite.

I_o is the minimum intensity of peak d, α is a factor modulating the increase in intensity as the polarization vector is changed, and γ shifts the \cos^2 curve. For example, for the vertical position, the fit parameters were $I_o = 0.06$, $\alpha = 0.08$, and $\gamma = 5.1$ with an R^2 of 0.99. A \cos^2 dependence has previously been observed for the carbonate oxygen and carbon π^* and σ^* peaks, which is expected when the angle between the polarization vector and the π^* or σ^* bond changes.^{3,23–26}

In contrast to the aragonite spectra, the calcite calcium L-edge spectra, shown in Figure 5, exhibit more distinct crystal field peaks and no polarization dependence. The spectra of Figure 5A have the six peaks characteristic of the calcite polymorph at the calcium L-edge and are for the crystal in the vertical orientation with the *c* axis in the $-z$ direction. Figure 5B emphasizes the lack of polarization dependence of the calcium spectrum by plotting the peak intensities for both sample orientations, obtained through peak fitting, of all 6 peaks as a function of beam polarization vector. The white line peaks at 352.6 eV (b2) and 349.2 eV (a2), respectively, are at a higher intensity than the peaks at 351.3 (b1), 348.0 (a1), 347.2 (1), and 346.9 (2), which is expected based on the intensity observed in the spectra in Figure 5A. While the peak intensities

vary slightly as the angle is changed, the variations are random and, except for the main L_2 and L_3 peaks, within the average variation observed in repeated spectra.

Figure 6 presents data extracted from a single, uniform region of a prismatic prism from *Pinctada margaritifera* as the beam polarization was varied. The spectra in Figure 6A show that the prism is calcitic, exhibiting the six peaks characteristic of the calcite polymorph, and that the spectra are independent of beam polarization, as the peak intensities and positions do not vary as the beam polarization varies. In Figure 6B, the peak-fitted height of the 351.3 eV peak (b1) is plotted as a function of the beam polarization vector, emphasizing the lack of polarization dependence of this peak in the calcite, biogenic, or geologic spectrum. As can be seen in Figure 6B, the peak height variations change randomly as the beam polarization vector is changed, and the variations are within the average variation observed in the repeated measurements at 0° and 90° .

In Figure 7, we present data acquired from a stack of nacre tablets co-oriented along the *c* axis and in the same field of view as the prismatic prism region in Figure 6, meaning the data presented in Figures 6 and 7 were acquired simultaneously. The spectra in Figure 7A indicate the nacre tablets are aragonitic, as

expected, with the spectra exhibiting the 6–7 peaks seen in the geologic aragonite spectrum of Figure 4A, with the number of apparent peaks depending on the beam's polarization vector. As seen in the geologic aragonite data in Figure 4A, the intensity of peak d at 351.3 eV varies as the beam polarization vector changes with respect to the sample. This is highlighted in the magnified version of Figure 7A, such that when the beam's polarization vector was at 0°, the peak d had its highest intensity and appears as a distinct peak, and when the beam's polarization vector was at 90°, peak d was at its lowest intensity and the spectrum appears to have only 6 peaks. It is important to emphasize that the orientation of the biogenic aragonite crystals is unknown and thus not expected to match either of the geologic aragonite sample orientations. Figure 7B plots the relationship between the height of peak d, determined through peak-fitting, and the beam's polarization vector with the data represented by black points and the best-fit curve by a red line. As with the geologic aragonite data, the best-fit curve is a cosine squared.

With the use of D_{4h} local symmetry, the calcium L₂₃ lines were calculated, as shown in Figure 8; there was minimal

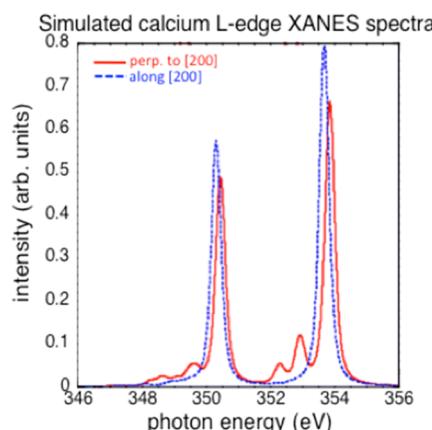


Figure 8. While simulations of the aragonite XANES spectrum do not perfectly match the experimental spectra, the polarization trends observed in the experimental data are roughly reproduced. Specifically, as shown in (A), when the polarization of the beam is aligned along the [100] of the aragonite crystal, the spectrum shows decreased intensity in the crystal field peaks (blue), while at an angle perpendicular to the [100], the crystal field peaks show an increased intensity (red). While the experimental spectra do not show all crystal field peaks changing in intensity as the angle between the polarization vector and the crystal is varied, they do show that the peak at 351.3 eV, peak d, changes in intensity as the polarization vector changes relative to the crystal, thus matching the trend observed in the simulated spectra shown here.

difference when the calculations were repeated with C_{4v} local symmetry. When the polarization is aligned perpendicular to [200], parallel to [001], there are two small peaks in the calculated multiplet structure (Figure 8) that are not present when the polarization vector is aligned along [200]. Although the spectra are not an exact match to the experimental spectra, the polarization dependence of the crystal field peaks is consistent with the experimental observation shown in Figure 4. The polarization dependence is also apparent from an analysis of the antibonding orbitals that are combinations of oxygen p and calcium d empty states (Figure 9A). The composition of an orbital aligned with a given Ca–O bond can be determined by examining the alignment between features in

the local p density of states on an oxygen atom and features in the Ca d density of states. From Figure 9A, it can be seen that there are two distinct distributions of the p density of states on the oxygen atoms, surrounding the calcium atoms shown in the structure of Figure 9B. The peak in the states indicated with an arrow matches a peak in the Ca d density of states just below the intense white line and also matches the position of peak d in the experimental spectrum.

The X-ray photoemission electron microscope (X-PEEM) maps presented in Figure 10 use the spectral results of Figures 4–9 to explore the structure of the nacre-prismatic boundary in a second *Pinctada margaritifera* sample. An X-PEEM map is acquired by taking two images acquired at different energies and dividing one by the other; this results in those areas with a high intensity of the numerator peak appearing white in the image and those areas with a low intensity of the numerator peak appearing dark in the image. The X-PEEM maps presented here, a carbon polarization-dependent imaging contrast (PIC) map (Figure 10A) and a calcium map (Figure 10B), are of the same region of the nacre-prismatic boundary from a cross section of the second *Pinctada margaritifera* sample. The carbon map, Figure 10A, created by a division of the π^* peak at 290.3 eV by the σ^* peak at 305 eV, indicates the alignment of the calcium carbonate crystal's c axis with the synchrotron beam's polarization vector, with the light crystals having their c axes aligned with the beam and the dark crystals having their c axes closer to 90° from the beam.^{3,4} Notice in Figure 10A the wide distribution of crystal orientations close to the nacre-prismatic boundary, near the right-hand side of the image, and that the crystals start out as prisms and eventually become nacre tablets. In Figure 10B, we present the exact same area, but with a calcium map, in which the 351.3 eV peak, peak d from Figure 7, was divided by the nonpolarization dependent pre-edge at 345 eV, resulting in those regions with high intensity 351.3 eV peaks appearing white and those with low 351.3 eV peak intensities appearing dark. As in Figure 10A, there is a distribution of gray levels near the nacre-prismatic boundary and within the nacre tablets, though the distribution of gray levels is not as large as that observed in Figure 10A. In addition, it is important to note that the nacre crystals do not necessarily appear with the same gray level in Figure 10B as they do in Figure 10A. Namely, some dark crystals from Figure 10A become lighter in Figure 10B than their neighbors that were lighter than them in Figure 10A, as indicated by the arrows.

DISCUSSION

The crystal field peaks in the calcium L-edge XANES spectra, specifically peaks 1, 2, a1, b1, and d, depend largely on the coordination symmetry of the calcium atom,^{12,13,19} which in turn depends on the local environment. For a crystal with the calcium atom in an octahedral coordination, such as observed in calcite, it is expected that there will be two small peaks before the a1 peak.^{12,13} In contrast, aragonite, in which the calcium has a 9-fold coordination to oxygen, the crystal field is expected to be much weaker.¹² These observations largely match up with the Ca L-edge XANES spectra presented in Figure 1, with the calcite and aragonite spectra having the two small peaks prior to a1, peaks 1 and 2, and the aragonite spectrum having weaker a1 and b1 peaks. However, they do not fully explain the spectral features as the observations leave out any explanation for the remaining peak, peak d, in the aragonite spectrum. The data presented here not only clearly shows that peak d is an inherent

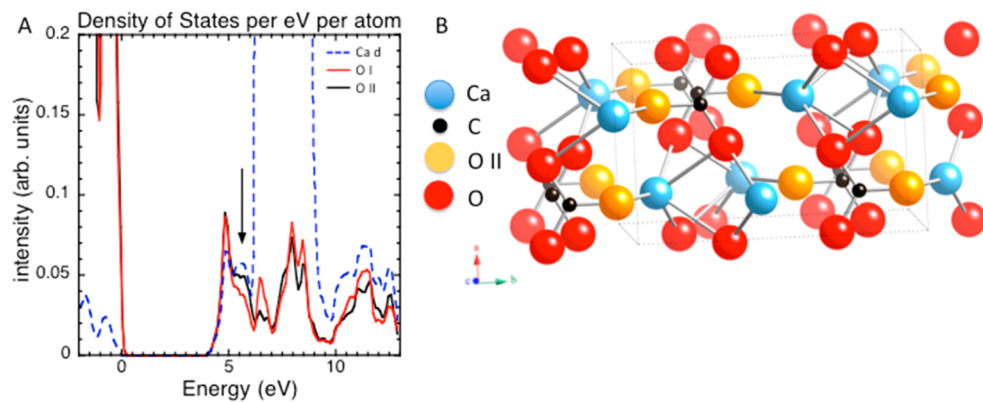


Figure 9. (A) The d density of states for calcium (blue dotted line) and oxygen p densities of states at 2 sites, labeled I and II (red and black, respectively). The states corresponding to the antibonding orbitals that are responsible for the feature marked peak d in the aragonite spectrum are marked with an arrow and is due to the bonding between the calcium (blue atoms) and the oxygen II (orange atoms) in the aragonite crystal structure shown in (B).

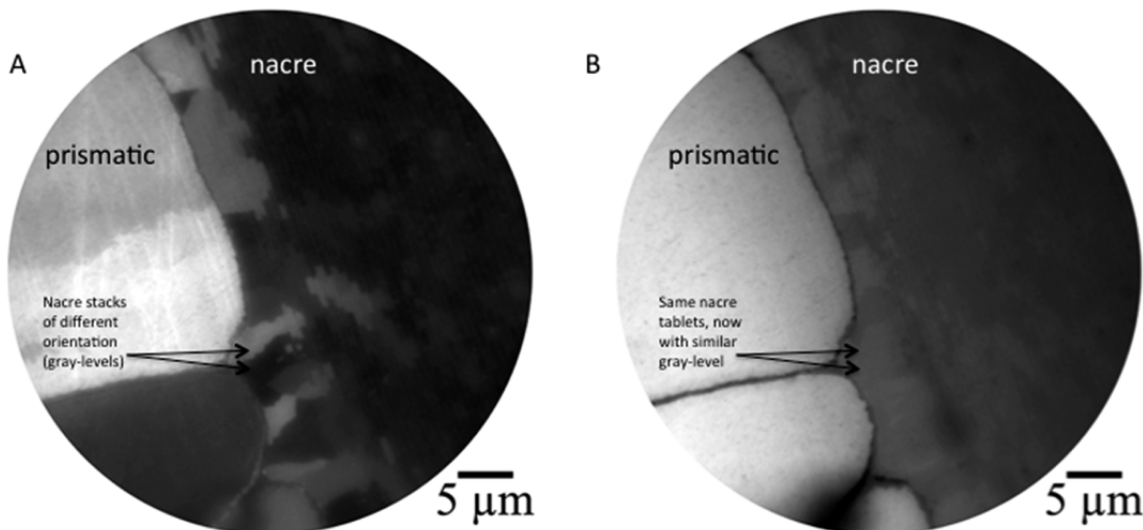


Figure 10. (A and B) X-ray photoemission electron microscopy (X-PEEM) maps of the nacre-prismatic boundary in *Pinctada margaritifera* obtained by dividing an image acquired at one peak (290.3 eV for A and 351.3 eV (peak d) for B) by a second image acquired at either a second peak (301.5 eV for A) or the pre-edge (343 eV for B). The map shown in (A) indicates the *c* axis orientation of each crystal through gray-level^{3,4,27} with those crystals with their *c* axes aligned with the polarization vector appearing white and those with their *c* axes misaligned with respect to the polarization vector appearing dark. The map in (B) supports the data in Figures 3–6, by showing that the prismatic region has a higher intensity 351.3 eV peak (as expected from peak b1 in the calcite spectrum) and that the aragonite nacre region exhibits polarization dependence (variations in gray levels), while the prismatic region does not. If you look closely at the two maps you will notice that not every region perfectly overlaps (one such region is indicated by the arrows), there are some regions that appear dark in the carbon map while appearing light in the calcium map.

part of the aragonite spectrum and not caused by calcite contamination of the aragonite crystal but also determines which bonds within aragonite contribute to peak d, enabling full usage of the aragonite calcium spectrum.

Experimentally, peak d in the aragonite spectrum is located at 351.3 eV, at the same energy as the peak, b1, in the calcite spectrum, which explains why peak d was previously attributed to calcite peak b1.¹² While the presence of peak d in almost all reported aragonite spectra is an indication that peak d is an inherent part of the aragonite spectrum, the fact that peak d is polarization-dependent confirms this point conclusively. Peak b1 in the calcite spectrum does not exhibit any polarization dependence, nor is any polarization dependence expected as calcite has octahedral symmetry.^{19,20} Peak d in the aragonite spectrum, on the other hand, does exhibit polarization dependence, varying as the orientation of the aragonite crystal's

crystallographic axes are changed with respect to the beam's polarization vector.

While the approximate tetrahedral symmetry used here is a crude representation of the local environment for Ca in aragonite, it does show the effect of polarization, enabling a full interpretation of the aragonite Ca L-edge spectrum. The density of states shown in Figure 9A suggests that there is an antibonding orbital that is a combination of the calcium d states and the p states on the closest oxygen atoms at a distance of 2.4 Å. Transitions to this antibonding orbital are responsible for the feature labeled d in the aragonite spectrum. The oxygen II atoms contributing to this effect are shown as orange in Figure 9B. As can be seen in the structure, Figure 9B, the bonds between the calcium atoms and oxygen II atoms are located in the *c*–*b* plane of the aragonite crystal, meaning that polarization dependence data can provide information regarding the orientation of the crystal's *c* and *b* axes relative to the

beam (see the Supporting Information). Figure 11 shows the simulated polarization dependence for the experimental

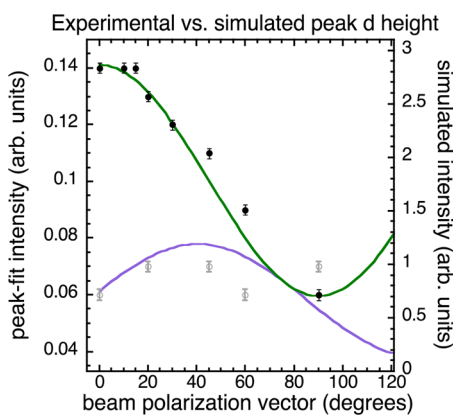


Figure 11. Using the crystal structure shown in Figure 10 in the configurations shown in Figure 2 (panels A and B), the polarization dependence experimentally observed (○ and ● circles) was reproduced via simulation (purple and green lines).

conditions described in Figure 2 (panels A and B), with the experimental data plotted in closed circles (vertical position, Figure 2B) and open circles (horizontal position, Figure 2A) and the simulated dependence as lines (green for vertical and purple for horizontal). The strong polarization dependence when the crystal is in orientation 2A in conjunction with weak calculated polarization dependence when the crystal is in orientation 2B supports the view that the antibonding orbital responsible for peak d is in the c–b plane, and there are no direct bonds between the Ca and O atoms in the a–c plane that are 2.64 Å apart.

By fully interpreting the aragonite calcium spectrum, we not only are able to use the distinct nature of the calcite and aragonite calcium L-edge spectra to distinguish between the calcitic and aragonitic regions in a biomineral sample (Figures 6 and 7), as done previously^{2,16,18,28} but also are able to use the polarization-dependent nature of the aragonite calcium spectrum to look at the microstructure of a biomineral sample (Figure 10). As the calcium polarization dependence depends on the location not only of the c axis, but also the b axis, calcium provides information that is complementary to previous polarization imaging contrast methods^{3,4,27} that probe solely the c axis of the given calcium carbonate crystal. Thus, using the oxygen or carbon polarization dependent imaging with calcium provides a more complete view of the biomineral microstructure by delineating which crystals are misaligned with respect to one another not only along the c axis but also along the b axis. This effect is presumably behind the differences in gray level that we observe between the carbon PIC map and calcium division map in Figure 10, with the carbon PIC map delineating relative orientation differences between the c axes of adjacent tablets and the calcium division map the relative orientation of both the c and b axes. To quantitatively determine orientation of individual nacre tablets, one would have to take images while changing the polarization vector with respect to the surface, and then repeat the process with the crystal rotated by 90°. Subsequent analysis using the eqs 1–6 in the Supporting Information could then be used to determine the angles quantitatively.

Finally, while we do not observe significant peak broadening when comparing the geologic and biogenic polymorphs, as seen

in synthetic systems,²⁹ we do observe that the polarization trends remain the same for both geologic and biogenic calcite and aragonite. Namely, biogenic calcite exhibits no polarization dependence while biogenic aragonite exhibits polarization dependence in peak d at 351.3 eV. The lack of peak broadening may be due to the fact that the organic fraction in the biomineral being examined, *Pinctada maragarifera*, is considerably less than that from the model biomineral in which peak broadening was observed.²⁹

CONCLUSIONS

We have shown, through a thorough analysis of the calcite and aragonite calcium L-edge XANES spectra, that the biogenic and geologic aragonite spectrum is polarization dependent while the biogenic and geologic calcite spectrum is not. In particular, a peak in the aragonite spectrum at 351.3 eV, peak d, which was previously attributed to calcite contamination, changes in intensity as the orientation of the aragonite crystal is varied with respect to the beam's polarization vector. This peak is due to an antibonding orbital between calcium and specific oxygen atoms within the aragonite structure that lie within the c–b plane. Due to the orientation of the bond within the aragonite structure, data taken at the Ca L-edge provides information about the orientation of the c and b axes within the aragonite crystal, both within geologic and biogenic samples. With future work, it will be possible to obtain a quantitative measurement of the c and b axes in biomimetics from the calcium L-edge. Thus, this information not only provides a definitive assignment and interpretation of the aragonite spectrum but also provides, most excitedly, a new tool for probing the orientation of microcrystals in aragonitic biomimetics.

ASSOCIATED CONTENT

S Supporting Information

Four tables, containing the peak-fitting coefficients for the experimental spectra, and calculations done showing that only the c and b axes can be determined from the polarization dependence of the aragonite spectrum. This material is available free of charge via the Internet at <http://pubs.acs.org>.

AUTHOR INFORMATION

Corresponding Author

*E-mail: rmetzler@colgate.edu.

Notes

The authors declare no competing financial interest.

ACKNOWLEDGMENTS

We thank the CLS beamline scientists, Chithra Karunakarn and Jian Wang, for their support during PEEM experiments. We thank Martin Wong for his helpful discussions about EBSD. Research described in this paper was performed at the Canadian Light Source, which is funded by the Canada Foundation for Innovation, the Natural Sciences and Engineering Research Council of Canada, the National Research Council Canada, the Canadian Institutes of Health Research, the Government of Saskatchewan, Western Economic Diversification Canada, and the University of Saskatchewan. This work was supported by Colgate University and NSF MRI Grant EAR-103979. P.R. is grateful for an Erna and Jakob Michael Visiting Professorship at the Weizmann Institute.

■ REFERENCES

- (1) Mann, S. *Biomineralization: Principles and Concepts in Bioinorganic Materials Chemistry*; Oxford University Press: Oxford, 2001.
- (2) Politi, Y.; Metzler, R. A.; Abrecht, M.; Gilbert, B.; Wilt, F. H.; Sagi, I.; Addadi, L.; Weiner, S.; Gilbert, P. U. P. A. Transformation Mechanism of Amorphous Calcium Carbonate into Calcite in the Sea Urchin Larval Spicule. *Proc. Natl. Acad. Sci. U.S.A.* **2008**, *105*, 17362–17366.
- (3) Metzler, R. A.; Zhou, D.; Abrecht, M.; Chiou, J. W.; Guo, J.; Ariosa, D.; Coppersmith, S. N.; Gilbert, P. U. P. A. Polarization-Dependent Imaging Contrast in Abalone Shells. *Phys. Rev. B* **2008**, *77*, 064110.
- (4) Metzler, R. A.; Abrecht, M.; Olabisi, R. M.; Ariosa, D.; Johnson, C. J.; Frazer, B. H.; Coppersmith, S. N.; Gilbert, P. U. P. A. Architecture of Columnar Nacre, and Implications for Its Formation Mechanism. *Phys. Rev. Lett.* **2007**, *98*, 268102.
- (5) Gilbert, P. U. P. A.; Metzler, R. A.; Zhou, D.; Scholl, A.; Doran, A.; Young, A.; Kunz, M.; Tamura, N.; Coppersmith, S. N. Gradual Ordering in Red Abalone Nacre. *J. Am. Chem. Soc.* **2008**, *130*, 17519–17527.
- (6) Gilbert, P. U. P. A.; Young, A.; Coppersmith, S. N. Measurement of C-Axis Angular Orientation in Calcite (CaCO_3) Nanocrystals Using X-Ray Absorption Spectroscopy. *Proc. Natl. Acad. Sci. U.S.A.* **2011**, *108*, 11350–11355.
- (7) Zhou, D.; Metzler, R. A.; Tyliszczak, T.; Guo, J.; Abrecht, M.; Coppersmith, S. N.; Gilbert, P. U. P. A. Assignment of Polarization-Dependent Peaks in Carbon K-Edge Spectra from Biogenic and Geologic Aragonite. *J. Phys. Chem. B* **2008**, *112*, 13128–13135.
- (8) DeVol, R. T.; Metzler, R. A.; Kabalah-Amitai, L.; Pokroy, B.; Politi, Y.; Gal, A.; Addadi, L.; Weiner, S.; Fernandez-Martinez, A.; Demichelis, R. et al. Oxygen Spectroscopy and Pic-Mapping of Calcium Carbonate Minerals and Biominerals, *J. Phys. Chem. B* **2014**, *10.1021/jp503700g*.
- (9) Killian, C. E.; Metzler, R. A.; Gong, Y. U. T.; Olson, I. C.; Aizenberg, J.; Politi, Y.; Wilt, F. H.; Scholl, A.; Young, A.; Doran, A.; et al. Mechanism of Calcite Co-Orientation in the Sea Urchin Tooth. *J. Am. Chem. Soc.* **2009**, *131*, 18404–18409.
- (10) Benzerara, K.; Menguy, N.; Obst, M.; Stolarski, J.; Mazur, M.; Tyliszczak, T.; Brown, G. E., Jr.; Meibom, A. Study of the Crystallographic Architecture of Corals at the Nanoscale by Scanning Transmission X-Ray Microscopy and Transmission Electron Microscopy. *Ultramicroscopy* **2011**, *111*, 1268–1275.
- (11) Benzerara, K.; Meibom, A.; Gautier, Q.; Kazmierczak, J.; Stolarski, J.; Menguy, N.; Brown, G. E., Jr. Nanotextures of Aragonite in Stromatolites from the Quasi-Marine Satonda Crater Lake, Indonesia. *Geological Society* **2010**, *336*, 211–224.
- (12) Fleet, M. E.; Liu, X. Calcium $L_{2,3}$ -Edge XANES of Carbonates, Carbonate Apatite, and Oldhamite (CaS). *Am. Mineral.* **2009**, *94*, 1235–1241.
- (13) Rez, P.; Blackwell, A. Ca L_{23} Spectrum in Amorphous and Crystalline Phases of. *J. Phys. Chem. B* **2011**, *115*, 11193–11198.
- (14) Effenberger, H.; Mereiter, K.; Zemann, J. Crystal Structure Refinements of Magnesite, Calcite, Rhodochrosite, Siderite, Smithonite, and Dolomite, with Discussion of Some Aspects of the Stereochemistry of Calcite Type Carbonates. *Z. Kristallogr.* **1981**, *156*, 233–243.
- (15) Caspi, E. N.; Pokroy, B.; Lee, P. L.; Quintana, J. P.; Zolotoyabko, E. On the Structure of Aragonite. *Acta Crystallogr.* **2005**, *B61*, 129–132.
- (16) Benzerara, K.; Yoon, T. H.; Tyliszczak, T.; Constantz, B.; Spormann, A. M.; Brown, G. E., Jr. Scanning Transmission X-Ray Microscopy Study of Microbial Calcification. *Geobiology* **2004**, *2*, 249–259.
- (17) Naftel, S. J.; Sham, T. K.; Yiu, Y. M.; Yates, B. W. Calcium L-Edge Xanes Study of Some Calcium Compounds. *J. Synchrotron Radiat.* **2001**, *8*, 255–257.
- (18) Obst, M.; Dynes, J. J.; Lawrence, J. R.; Swerhone, G. D. W.; Benzerara, K.; Karunakaran, C.; Kaznatcheev, K.; Tyliszczak, T.; Hitchcock, A. P. Precipitation of Amorphous CaCO_3 (Aragonite-Like) by Cyanobacteria: A Stxm Study of the Influence of Eps on the Nucleation Process. *Geochim. Cosmochim. Acta* **2009**, *73*, 4180–4198.
- (19) de Groot, F. M. F.; Fuggle, J. C.; Thole, B. T.; Sawatzky, G. A. $L_{2,3}$ X-Ray Absorption Edges of D0 Compounds: K^+ , Ca^{2+} , Sc^{3+} , and Ti^{4+} in Oh (Octahedral Symmetry). *Phys. Rev. B* **1990**, *41*, 928–937.
- (20) Himpel, F. J.; Karlsson, U. O.; Morar, J. F.; Rieger, D.; Yarmoff, J. A. Determination of Interface Surfaces for $\text{CaF}_2/\text{Si}(111)$ from near-Edge X-Ray-Absorption Measurements. *Phys. Rev. Lett.* **1986**, *56*, 1497–1500.
- (21) De Stasio, G.; Frazer, B. H.; Gilbert, B.; Richter, K. L.; Valley, J. W. Compensation of Charging in X-Pem: A Successful Test on Mineral Inclusions in 4.4 Ga Old Zircon. *Ultramicroscopy* **2003**, *98*, 57–62.
- (22) Kresse, G.; Furthmüller, J. Efficient Iterative Schemes for Ab Initio Total-Energy Calculations Using a Plane-Wave Basis Set. *Phys. Rev. B* **1996**, *54*, 11169–11186.
- (23) Madix, R. J.; Solomon, J. L.; Stohr, J. The Orientation of the Carbonate Anion on $\text{Ag}(110)$. *Surf. Sci.* **1988**, *197*, L253–L259.
- (24) Stohr, J. *Nexafs Spectroscopy*; Springer-Verlag: Berlin, 1992.
- (25) Leapman, R. D.; Silcox, J. Orientation Dependence of Core Edges in Electron-Energy-Loss Spectra from Anisotropic Materials. *Phys. Rev. Lett.* **1979**, *42*, 1361–1364.
- (26) Leapman, R. D.; Fejes, P. L.; Silcox, J. Orientation Dependence of Core Edges from Anisotropic Materials Determined by Inelastic Scattering of Fast Electrons. *Phys. Rev. B* **1983**, *28*, 2361–2373.
- (27) Gilbert, P. U. P. A.; Young, A.; Coppersmith, S. N. Measurement of C-Axis Angular Orientation in Calcite (CaCO_3) Nanocrystals Using X-Ray Absorption Spectroscopy. *Proc. Natl. Acad. Sci. U.S.A.* **2011**, *108*, 11350–11355.
- (28) Hanhan, S.; Smith, A. M.; Obst, M.; Hitchcock, A. P. Optimization of Analysis of Soft X-Ray Spectromicroscopy at the Ca 2p Edge. *J. Electron. Spectrosc. Relat. Phenom.* **2009**, *173*, 44–49.
- (29) Metzler, R. A.; Tribello, G. A.; Parrinello, M.; Gilbert, P. U. P. A. Asprich Peptides Are Occluded in Calcite and Permanently Disorder Biominerals Crystals. *J. Am. Chem. Soc.* **2010**, *132*, 11585–11591.